Subcooled Boiling Oscillations in Natural Circulation Boiling Loop at Low Pressure

Arnab Karmakar, Nababithi Goswami, and Swapan Paruya
Dept. of Chemical Engineering, NIT Durgapur, West Bengal 713209, India

DOI 10.1002/aic.14258
Published online October 28, 2013 in Wiley Online Library (wileyonlinelibrary.com)

Flow instabilities in a natural circulation boiling loop at a low pressure are reported. The oscillations at boiling incipience are primarily chaotic and bifurcate to quasiperiodic ones depending on inlet subcooling ΔT_{sub} and heater power Q. They also strongly depend on water volume Φ in the loop. We have presented power spectrums, attractor reconstructions, and Hurst exponents for the analysis of the experimental data. The analysis shows that the primary oscillations are very similar to geysering instability. Chaotic oscillations occur at low ΔT_{sub} or high Q, whereas quasiperiodic oscillations occur at high ΔT_{sub} or low Q. Our experiments also suggest that wall superheat exceeding a critical value triggers the instability. © 2013 American Institute of Chemical Engineers *AIChE J*, 60: 375–386, 2014
Keywords: multiphase flow, nuclear engineering, subcooled boiling, flow instability

Introduction

Natural circulation boiling loop (NCBL) has extensive applications in boiling water reactors (BWRs), drum-type boilers, thermosyphon reboilers in distillation column and chemical evaporator, thermosyphon-based heat removal from chemical reactors, and so forth. Studies on thermal hydraulics in these applications have received significant attention in regard to safe and optimal operations. The performance of a thermosyphon process is strongly coupled with the loop flow rate (circulation rate) W_{loop} as a result of density difference caused by the application of heat. The natural circulation systems offer better operational safety compared to forced circulation systems. For example, the natural circulation-based heat removal such as passive cooling avoids melting of fuel rods in nuclear power plants in the post-loss of coolant accident (LOCA) situations. The failure of the primary cooling pump may result in severe consequences. However, because of low driving heads, they suffer from several nonlinear flow instabilities classified by Boure et al.[1] Experimental studies report five major instabilities in NCBL at low pressures and low heat fluxes (Ledinegg,[2] Wissler et al.,[3] Chexal and Bergles,[4] Fukuda and Kobori,[5] Aritomi et al.,[6] Wang et al.,[7] Jiang et al.,[8] Kyung and Lee,[9] Hsieh et al.[10], Nayak et al.,[11] and Paruya and Bhattacharya[12]). The instabilities are flow excursion or flow reversal, geysering instability, natural circulation oscillation, flashing-induced instability, and Type I density-wave oscillation (DWO). Ledinegg first successfully analyzed the excursive instability that occurs when the curve of steady-state pressure drop of a boiling channel vs. flow rate (internal characteristic of the channel) has a negative slope. Wissler et al. reported periodic oscillations of W_{loop} and fluid temperature in flashing-induced instability in NCBL. This instability is similar to Type I DWO. In Type I DWO, the oscillations of temperature in the boiling region and the nonboiling region have phase difference and the oscillation periods are nearly equal to the transit time of fluid in chimney. Chexal and Bergles reported the static instability as periodic formation of small bubbles at high heat flux and high subcooling that favor the occurrence of chugging-type instability. The chugging is associated with the periodic expulsion of liquid from the channel due to very fast growth of vapor slug. Fukuda and Kobori observed two modes of DWOs in an NCBL (Type I and Type II) based on the steam quality of flow. Boure[13] reported that DWOs are of low frequencies (less than 1.0 Hz) and originate due to transportation delays of the fluid in the flow channel.

Aritomi et al. reported geysering instability induced by condensation in NCBL. The geysering period reported by them strongly depends on boiling delay. Kyung and Lee experimentally observed periodic flow excursion in the loop at a low loop pressure p_{loop}. Wang et al. reported dominant frequency of 0.02 Hz in geysering in NCBL at low p_{loop}, low heater power Q and high inlet subcooling ΔT_{sub}. Jiang et al. also experimentally observed the geysering to occur at both regular and irregular frequencies of high magnitude due to the combined effect of self-evaporation and flashing instability. Nayak et al. experimentally detected two distinct unstable zones depending on Q in a multichannel NCBL at low p_{loop}. The unstable zones correspond to Type I DWOs at low Q and Type II DWOs at high Q. They also found that the amplitude of oscillations increased with Q until Q was increased to a critical value and then the amplitude decreased with Q. Paruya and Bhattacharya[12] identified the periodic pulses of both void fraction α and temperature in a natural circulation evaporator at low p_{loop} and low Q. Hsieh et al. observed different modes of flows including the steady flow (less than 150 kg/h), periodic flow of a medium amplitude (the peak value varied from 150 to 300 kg/h), periodic

Correspondence concerning this article should be addressed to S. Paruya at swapanparuya@gmail.com.

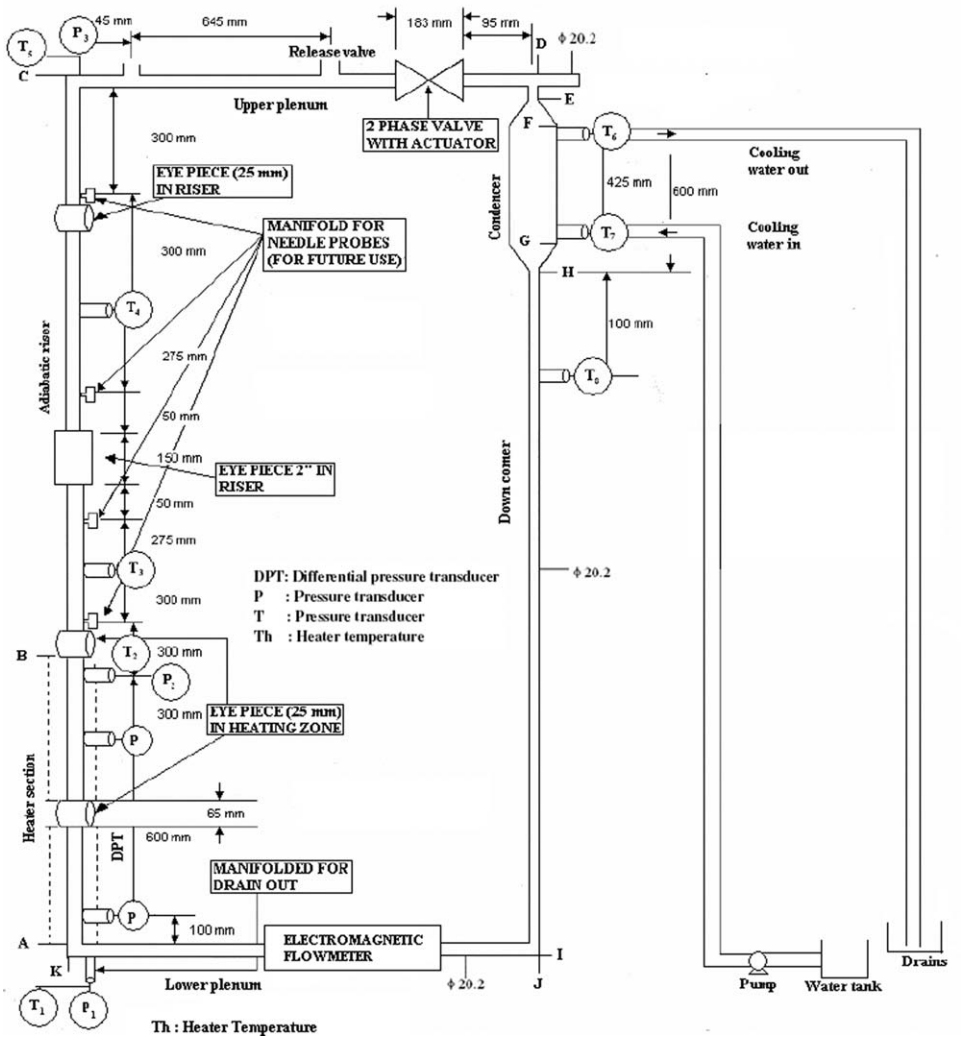

Figure 1. Schematic of our experimental NCBL.

flow of large amplitude (the peak value was greater than 300 kg/hr), and chaotic flow depending on Q and ΔT_{sub}. Marcel et al.[14] also reported geysering and flashing-induced instability at low Q and low p_{loop} in one and two-parallel channels. They also found flashing-induced oscillations having some characteristics of DWO.

From the above survey of literatures, we realize that the flow instabilities in NCBL at low p_{loop}, low Q, and high ΔT_{sub} are very complex because of many thermohydraulic feedbacks. Accurate identifications of the same have been always challenging field of research. Particularly, the understandings of the instabilities in NCBL at boiling incipience in subcooled boiling are not complete. Here, we extend the studies of Paruya et al.[15] rescaling the NCBL with a longer riser and a longer heated section (HS). Our experimental setup also differs from the existing ones with respect to the scaling ratio of NCBL. The existing loops reported in the literatures have longer riser (the ratio of the riser length to the HS-length Ω is 3.0–4.0) compared to ours ($\Omega = 2.0$). We also attempt to formulate a mechanism of the flow oscillations in NCBL at boiling incipience under varied conditions of Q and ΔT_{sub}. The effects of Q and ΔT_{sub} on the oscillations have been examined by the rigorous analysis of the time series using fast Fourier transform, time delay embedding, and Hurst exponent. In our experimental range of Q and ΔT_{sub}, flashing of liquid in the riser and the heater was not significant, although all the experiments were carried out at a low p_{loop} of 111.325 kPa.

Experimental Setup and Procedure

Figure 1 shows the schematic of our experimental two-phase NCBL. The NCBL mainly consists of six sections—HS, adiabatic riser, condenser, down comer (DC), upper plenum, and lower plenum. The sizes of the various parts of the loop are given in Table 1. The NCBL-geometry is based on the loop of Hsieh et al.[10] with a different scaling ratio. The horizontal plenums connect the hot leg and the cold leg of the loop. The condenser in the loop is a water-cooled shell-and-tube heat exchanger with four tubes. The hot fluid from the riser is cooled on the shell side of the condenser. The rectangular loop was fabricated of SS 316. Different parts of the loop are manifolded to fit temperature sensors and pressure sensors. Eight resistance temperature detectors (RTDs) T_1–T_8 made of SS-310 with the range of 0–400°C are used to measure temperatures. Three pressure sensors P_1–P_3 made of SS-310 (WIKA make, Germany) are placed at heater inlet, heater outlet, and the top of the riser. T_1–T_8 and P_1–P_3

Table 1. Dimensions of the Various Sections of the NCBL

Section	Orientation	Diameter (m)	Length (m)
Heated section (AB)	Vertical	0.02096 (ID) 0.02671 (OD)	1.00
Adiabatic riser section (BC)	Vertical	0.02096 (ID) 0.02671 (OD)	2.00
Upper plenum (CD)	Horizontal	0.02096 (ID) 0.02671 (OD)	1.20
Lower plenum (JK)	Horizontal	0.02096 (ID) 0.02671 (OD)	1.20
Condenser (EH)	Vertical	–	0.60
Condenser tubes (4 Nos., FG)	Vertical	0.010 (ID)	0.45
Down comer (HI)	Vertical	0.02096 (ID) 0.02671 (OD)	2.35

are indicated in Figure 1. The loop pressure is controlled at the exit of the riser. The differential pressure transmitter made of SS-310 with the range of 0–10 bar is placed across the distance of 0.6 m in the HS to measure the pressure drop. The electromagnetic flow meter (EFM) with 20-mm polytetrafluoroethylene lining and the range of 0–1.8 m^3/h is placed at the midpoint of the lower plenum to measure the loop flow. For accurate measurements, no magnetic material should be kept near the EFM as the material induces the magnetic field of the EFM. The advantage of using EFM is that it can accurately measure very low flow as well as reverse flow experienced in our NCBL. A two-phase valve controlling overall loop resistance is placed on the upper plenum to regulate the loop flow rate.

The NCBL also has the cold-leg temperature controller (CLTC), pressure controller (PC), and heater power controller for regulating ΔT_{sub}, p_{loop}, and Q, respectively. To maintain the desired cold-leg temperature, CLTC was operated in the proportional-integral (PI) mode manipulates the cooling water flow to the condenser. The PI controller may lend the possibility of more intense system oscillations because of its oscillatory nature. We noted that the controlled variable such as cold leg temperature was oscillating with very small amplitude of 2.62°C at a low ΔT_{sub} of 30°C. This introduces a small amount of uncertainty in oscillations. p_{loop} is controlled in proportional mode by manipulating air injection through a solenoid valve on the line connecting the loop and a compressor. For uniform and safe heating, six segmental heater-coils (Kanthal super: $MoSi_2$) are wound around the aluminum tube of the heater length. The aluminum tube is coaxially placed outside the heated pipe. In the annular section, the heat is transferred by radiation and convection. An accurate control of the heater power is achieved by a thyristor power controller in PID mode.

The loop was filled up with distilled water (prepared by the ultraquartz distiller) as the working fluid. The data logger and supervisory control and data acquisition (SCADA) were put online with the sensors and controller. The heater was then put on for heating the water in the loop.

Table 2 shows the rates of rise of wall temperature and fluid temperature at different Q. It was observed that two-phase flow incepted in the HS at nearly atmospheric pressure (111.325 kPa) when the cold-leg temperature (at the exit of the condenser) attains 65°C. The pump was then run for cooling water flow in the condenser. It was noted that the temperature controller performs better at a high Q and a high ΔT_{sub}. At a given Q, the experiments were carried out at different cold-leg temperatures of 70, 60, and 50°C (corresponding to ΔT_{sub} of 30, 40, and 50°C, respectively) to study the effect of ΔT_{sub}. The controller parameters need to be tuned repeatedly because of more oscillatory response of the condenser at the lower ΔT_{sub}. The time series of temperatures from the sensors T_1–T_8, pressures from the sensors P_1–P_3 and W_{loop} from EFM were recorded when the heating of water was initiated. The data logger software stores the data from all sensors via SCADA panel @ 0.5 Hz. The controllers were tuned online whenever needed. The operating conditions in our experiments have been presented in Table 3. Note that the two-phase valve controlling the loop resistance was kept fully open in all experiments. Total pressure-loss coefficient of the loop including bends, EFM, condenser, and valves is 38.34.

Table 2. Heating Rate of Heater Wall and Loop Fluid at Different Heating Power

Heating Power (kW)	Wall Temperature Rise (°C/min)	Fluid Temperature Rise (°C/min)
3.0	0.48	0.18
4.0	1.92	1.14
5.0	2.28	1.56

It is required to mention measurement uncertainties and experimental uncertainties in this study. All the instruments including pressure sensors, RTDs, and EFM have uncertainties less than 0.5%. The standard deviations of loop flow rate and inlet pressure for a number of sets of experiments at all conditions differ within ±10.0 and ±8.0%, respectively. These uncertainties are due to the controllability of CLTC and the loop PC. There is also a small loss of water from the loop and air injection into the loop for the control of p_{loop}. The fluctuations of cold leg temperature in CLTC are ±2.62°C at $\Delta T_{sub} = 30$°C, ±1.71°C at $\Delta T_{sub} = 40$°C, and ±1.47°C at $\Delta T_{sub} = 50$°C while the loss of water for 1-h experiment varies in between 1.5 and 5.0%. Also, note that all the controllers have uncertainties within 0.5% of full scale. The uncertainties show that the controllers perform better at high ΔT_{sub}. On the other hand, the signals of loop flow rate and inlet pressure under analysis presented in the following sections are a bit nonstationary. For a purely homogeneous (stationary or sustained oscillation) signal, the standard deviation is independent of the time. In this context, the uncertainties at the conditions are within ±12% based on the computation of the standard deviation varying with time.

Results and Discussion

In this section, we discuss the effect of Q and ΔT_{sub} on the flow oscillations and the power spectral analysis of the

Table 3. Operating Conditions of the Experiments

Data Set	Loop Pressure p_{loop} (kPa)	Heater Power Q (kW)	Heat Flux q'' (kW/m^2)	Inlet Subcooling ΔT_{sub} ($= T_{sat} - T_{in}$) (°C)
P1Q3DTSUB50	111.325	3.0	45.559	50.0
P1Q3DTSUB40				40.0
P1Q3DTSUB30				30.0
P1Q4DTSUB50		4.0	50.955	50.0
P1Q4DTSUB40				40.0
P1Q4DTSUB30				30.0
P1Q5DTSUB50		5.0	75.932	50.0
P1Q5DTSUB40				40.0
P1Q5DTSUB30				30.0

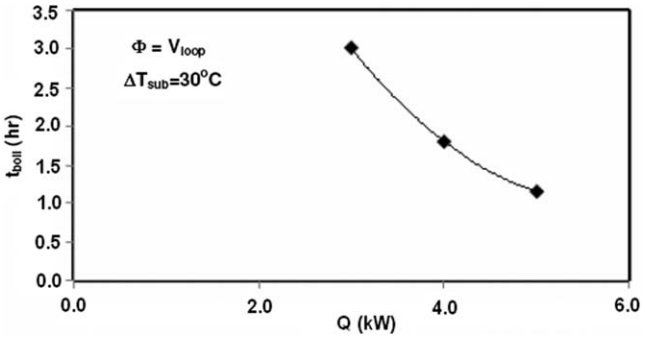

Figure 2. Variation of the time required for inception of boiling flow oscillations.

oscillations. One may note that the zero time shown in the plots is at the instant of the inception of flow oscillations. We noted that t_{boil} (the time required for the inception of the oscillations) at a given ΔT_{sub} strongly depends on Q. Figure 2 shows a nonlinear variation of t_{boil} with Q at $\Delta T_{sub} = 30°C$ for a given initial liquid volume $\Phi = V_{loop}$ (the loop is completely filled); V_{loop} is total volume of the loop. The variation gives the knowledge of the time required for attaining the oscillating conditions. It is obvious that the loop quickly attains the oscillating conditions due to the decrease of both Φ and ΔT_{sub}. In our experiments, the flow oscillations in the NCBL are due to mostly thermodynamic reasons.

The effect of Φ on the oscillations has been found to be significant. Flow oscillations with more reverse flow occur for a small decrease in Φ. It clearly indicates that the oscillations are very sensitive to gravitational force at the condition of low steam quality (highly subcooled condition). Figures 3a, b compare the amplitude of W_{loop}-oscillations at $Q = 4$ kW and $\Delta T_{sub} = 50°C$ when Φ was varied. The standard deviation of loop flow rate is 58.57 for 100% fill ($\Phi = V_{loop}$) and is 56.91 for 80% fill ($\Phi = 0.8V_{loop}$). The amplitude of W_{loop}-oscillations does not change appreciably. However, a larger amount of reverse flow is observed in the case of 80% fill. This is due to the greater increase of heater inlet pressure p_{Hi}. The local pressure fluctuation, on the other hand, gives the measure of the bubble behavior. Bubble growth and bubble expansion are facilitated by the lower hydrostatic head available at 80% fill. The standard deviation of the dimensionless heater inlet pressure p_{Hi}^{+} at 80% fill is significantly higher than that at 100% fill (0.031 in the former and 0.019 in the later). It means that the amplitude of p_{Hi}-oscillations is appreciably higher at 80% fill. From the power spectrums of the loop flow rate and p_{Hi} presented in Figure 4 in the both cases, we note that the case of 80% fill is quasiperiodic (the dominant frequencies and their harmonics of 0.022, 0.044, 0.066, and 0.088 Hz are present), whereas the case of 100% fill is almost periodic (no harmonics is present). The dominant frequency is less and the power of p_{Hi} is appreciably higher (about eight times) for 80% fill.

Effect of heater power on the flow oscillations

In this section, we discuss the effect of Q on the oscillations of W_{loop}, p_{Hi} and heater outlet temperature T_{Ho} at a given ΔT_{sub}. Chaotic oscillations are observed at a high Q, whereas quasiperiodic oscillations are observed at a low Q. Figures 5a and 6a, b present the oscillations of W_{loop} at $Q = 3$, 4, and 5 kW, respectively, for a given ΔT_{sub} of 50°C. The maximum values of W_{loop}-peaks (172.95, 172.90, and 175.90 kg/h at the respective Q) remain almost unaffected with increasing Q. The number of the large peaks of the oscillations increases with Q and so is the dominant frequency. From the power spectrums of W_{loop}, we noted the dominant frequencies of 0.029, 0.035, and 0.042 Hz at $Q = 3$, 4, and 5 kW, respectively. This shows that increase of the frequency of W_{loop} with Q is approximately linear.

Reverse flow and flow termination

Interestingly, we note a nonlinear increase of the extent of reverse flow or flow termination (flow rate decreases to zero) when Q is increased. The same are shown in Figures 5a and 6a, b. The minimum values of W_{loop} are -35.4, -44.34, and -69.47 kg/h at $Q = 3$, 4, and 5 kW, respectively. This reverse flow or flow reduction has a strong relation to the extent of bubble formations and condensations. At the peak of W_{loop}, the liquid temperature in the HS shown in Figure 5a starts to fall as the heated surface cools down and bubbles start to collapse in the HS. The bubble collapse also takes place in the riser where the liquid is still subcooled and a thermal-nonequilibrium condition exists. The condensation initiates the reverse flow from the riser to the HS and the flow reduction. Video imaging of tracer movements and our direct observation through the view glass (located at the exit of the HS) confirm that bubble condensation takes place. The tracer becomes stagnant or moves back to the HS from the riser. Increase in heater outlet temperature T_{Ho} (refer Figure 5a), decrease in pressure drop across the heater Δp_H, increase in p_{Hi} (refer Figure 5b), and negative W_{loop} are the signature of the reverse flow. Flow termination or reverse flow in NCBL at low pressures was also observed by Jiang et al.[8] and Hsieh et al.[10] In our experiments, the extent of the flow termination or flow reversal at a relatively low Q is more due to the scaling ratio of our NCBL-geometry being

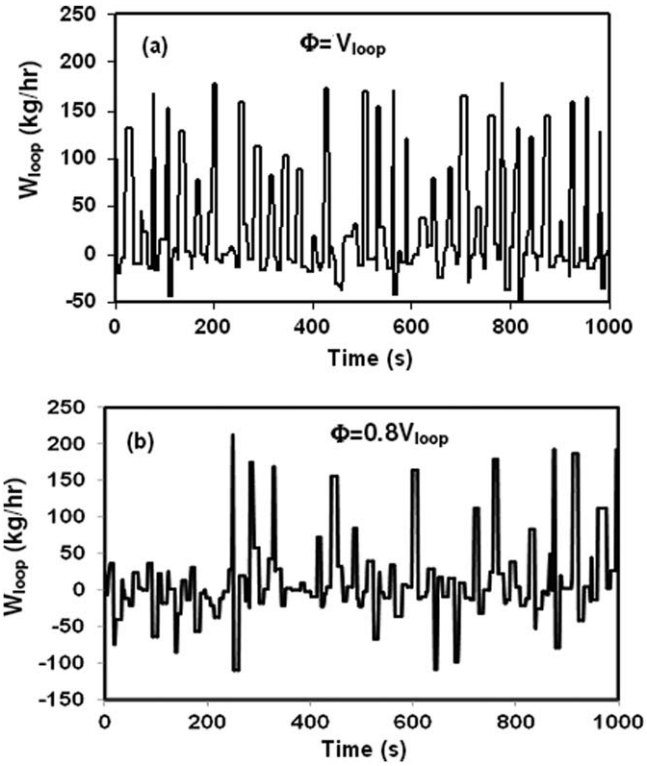

Figure 3. Effect of water content in the loop on oscillations of W_{loop} at $\Delta T_{sub} = 50°C$ and $Q = 4$ Kw.

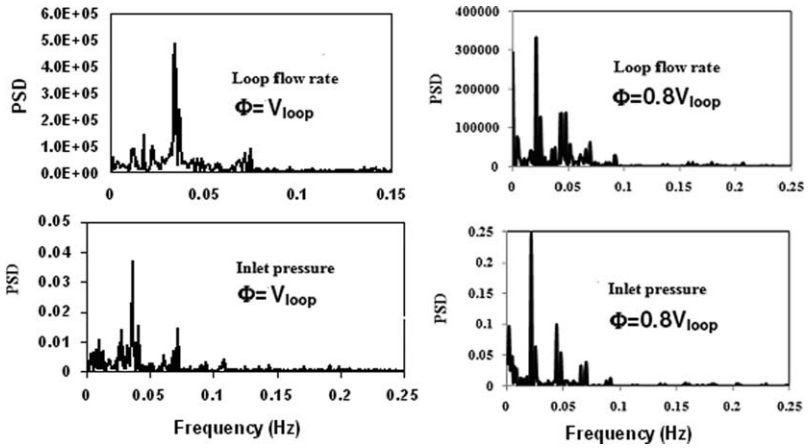

Figure 4. Effect of water content on the frequency and amplitude of oscillations at $\Delta T_{sub} = 50°C$ and $Q = 5$ kW.

different from theirs. Lower Ω of our loop compared to theirs imparts to the extended reverse flow because of lower hydrostatic head and lower frictional resistance. The time interval between two consecutive violent bubble formations was noted to be approximately equal to the time period of the flow oscillations. Some small peaks are present between two large peaks of W_{loop} at lower Q (see Figures 6a, b). The small peaks are due to the small bubbles formed at low wall superheat ΔT_{sat} ($T_l - T_{sat}(p)$, T_l is the temperature of liquid film adhered to the heater surface). T_l is usually assumed to be the heater-surface temperature T_w. Note that ΔT_{sat} increases with Q.

Thermodynamic origin of the oscillations

In this section, we confirm the thermodynamic reasons behind the occurrence of the flow oscillations. From direct observation and high-speed photography in the HS, we understand that the voids start to form near the exit of the HS. The heated single-phase liquid flows up to the region of lower hydrostatic head (lower saturation temperature) near the exit of the HS and becomes superheated. It results in the formation of voids and thereby the hydrostatic head further decreases. Consequently, bubbles form violently; the flow regime changes from bubbly one to slug one or churn one. The bubble growth and bubble expansion expel the steam-water mixture in a jet form. Interestingly, the oscillations are very similar to the geysering instability that occurs at the boiling incipience in a vertical channel at low Q, low p_{loop}, and high ΔT_{sub}. The classical geysering in a vertical channel is characterized by periodic water jets (geyer) from the channel. The jet is initiated by the bubble formation and its expansion. The water ejection results in decrease of hydrostatic head that causes vigorous boiling and more geysers form.

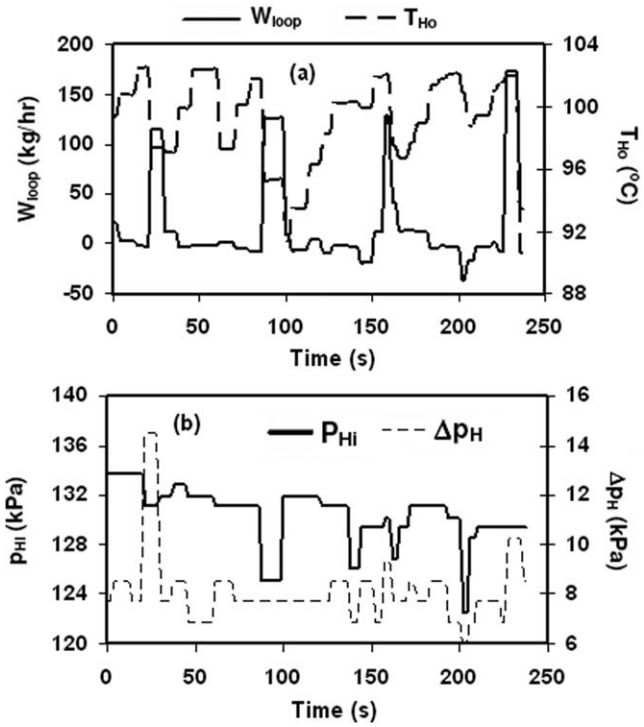

Figure 5. Oscillations at $Q = 3$ kW and $\Delta T_{sub} = 50°C$ (a) W_{loop} and T_{Ho} (b) P_{Hi} and Δp_H.

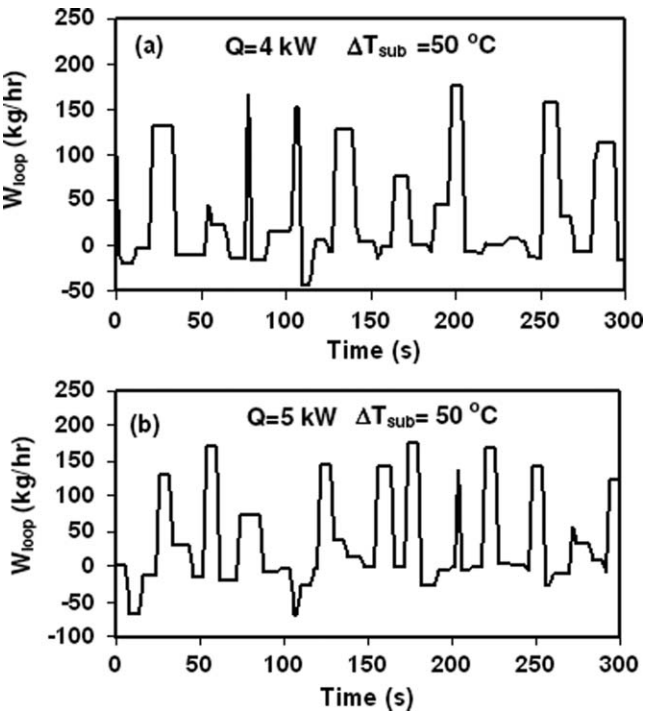

Figure 6. Effect of Q on oscillations of W_{loop} at $\Delta T_{sub} = 50°C$.

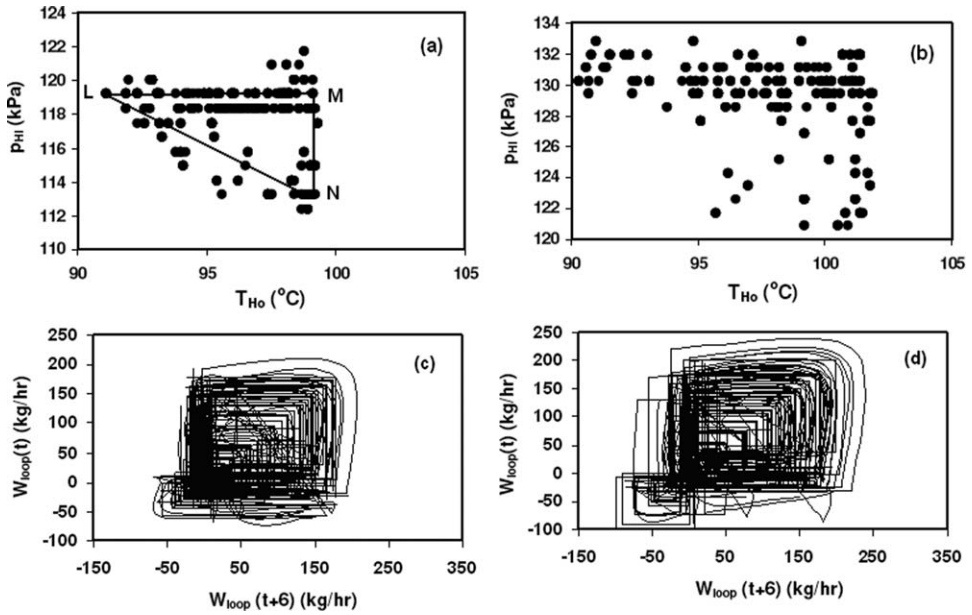

Figure 7. Phase portraits of P_{Hi}-T_{Ho} at $\Delta T_{sub} = 50°C$ and (a) $Q = 4$ Kw.(b) Q = 5 kW; reconstructed attractors of W_{loop} at $\Delta T_{sub} = 50°C$ and (c) Q = 4 kW (d) $Q = 5$ kW

However, a cycle of the observed geysering oscillations consists of three stages, as also reported by Yadigaroglu[16] and Paruya et al.[15] The stages of the cycle LMNL (symbolically denotes a cycle for geysering) are shown in the phase portraits of p_{Hi}-T_{Ho} presented in Figures 7a, b. The points L, M, and N form a triangular shape. The shape at 4 kW (Figure 7a) is more regular compared to that at 5 kW (Figure 7b). The horizontal line LM of the LMNL represents the incubation stage (heating at a constant pressure to nucleation point); the vertical line MN is expulsion stage (sudden decrease of static head due to nucleation aggravating boiling followed by the bubble growth to slug formation). The diagonal line NL is refilling stage (gradual increase of static head due to bubble condensation in the riser causing low flow or reversed flow). Unlike the geysering instability of a periodic nature observed by Yadigaroglu[16] and Paruya et al.,[15] the present experiments support that the geysering periods are not purely periodic. It is also noted in Figures 7a, b that the chaotic geysering-oscillations become stronger as Q increases. The frequencies are more irregular at $Q = 5$ kW (the points in the phase portrait are more scattered). To confirm it further, the phase space for W_{loop}-time series has been reconstructed using Takens time delay embedding theorem.[17] The optimal time delay required for the reconstruction has been estimated to be 6.0 s using the method of Leibert and Schuster.[18] The reconstructed attractors at 4 and 5 kW presented in Figures 7c, d, respectively, show more chaotic nature of the oscillations at 5 kW. The reconstructed attractors at 5 kW are also more scattered. Thus, the chaotic phenomena are of higher dimension at higher Q. Although Jiang et al.[8] reported geysering instability of irregular frequencies, their study did not reveal sufficient insight of the chaotic behavior. We have described the chaotic behavior in details later through the estimation of Hurst exponents.

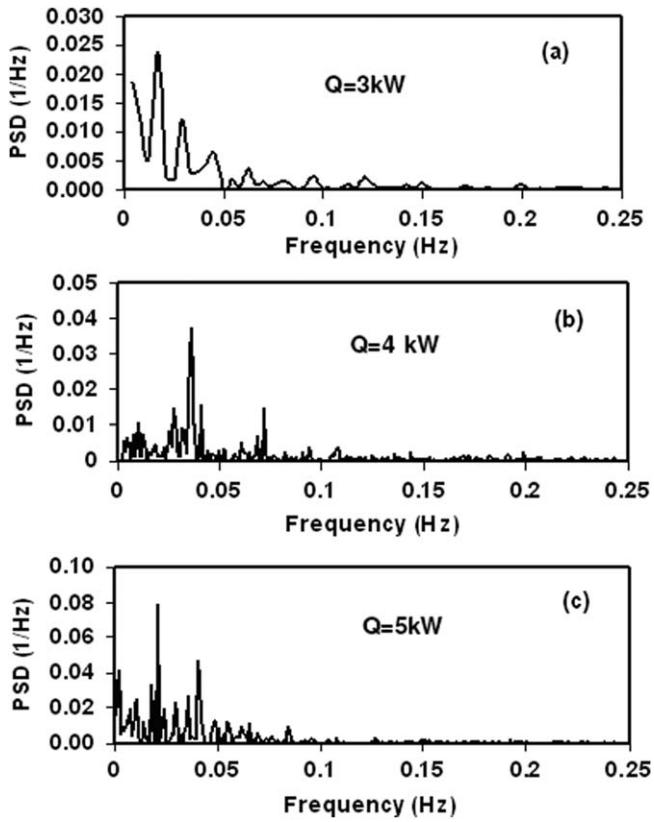

Figure 8. Effect of Q on PSDs of heater inlet pressure at $\Delta T_{sub} = 50°C$.

To demonstrate more precisely the effect of Q on the oscillations of p_{Hi}, power spectral densities (PSDs) of the dimensionless heater inlet pressure $p^{+}_{Hi}(p_{Hi}/p_{loop})$ at $Q = 3$, 4, and 5 kW at $\Delta T_{sub} = 50°C$ based on fast Fourier transform are presented in Figures 8a–c, respectively. The oscillations have dominant (primary) frequencies and secondary frequencies. Note that the dominant frequency and the secondary frequencies are the fundamental frequencies. The oscillations at $Q = 3$ kW seem to have a dominant (primary) frequency of 0.0167 Hz and a secondary frequency of 0.029 Hz, although they are very weak. At higher Q (4 and 5 kW), the oscillations look more irregular with distinct and higher

Table 4. Effect of Heater Power on the Frequency of Oscillations at $\Delta T_{sub} = 50°C$

Heater Power (kW)	4.0				5.0			
Strength (Hz^{-1})	0.0375	0.0154	0.0110	0.014	0.0785	0.0334	0.025	0.041
Fundamental frequency (Hz)	0.036	0.041	0.010	0.028	0.021	0.018	0.011	0.002
Harmonic frequency (Hz)	0.072	0.082	0.019	0.058	0.041	0.036	0.024	–
Harmonic frequency (Hz)	0.108	0.122	0.032	0.082	0.062	0.055	0.03	–

peaks. These high peaks indicate that the bubbles at higher Q are relatively big. The size distributions of the bubbles become wider at higher Q as we see many fundamental frequencies (peaks). Table 4 clearly presents the fundamental frequencies and their harmonics at $Q = 4$ and 5 kW. Figure 8 also shows the same. However, they clearly indicate wider distributions of bubble sizes and shapes at higher Q, leading to a complex bubble dynamics. The oscillations at a higher Q are, therefore, more chaotic. It is also important to mention that the gravitational effect (the effect of hydrostatic pressure drop) at a low Q is significant compared to the frictional pressure drop. The effect of fluid friction is more pronounced in a high steam-quality flow obtained at a high Q and at a low ΔT_{sub}. The friction effect causes the dominant frequency to reduce. For example, our estimation indicates that the frictional pressure drop increases to 44% (of total pressure drop at the maximum void) from 13% when ΔT_{sub} is decreased to 30°C from 50°C at $Q = 4.0$ kW. The acceleration part is found to be negligible.

Finally, the power spectrums of p_{Hi}^{+} confirm that the oscillations are due to the thermodynamic effect involving the fluctuations of the local pressure, which eventually induces the hydrodynamic effect leading to vigorous oscillations with decrease of ΔT_{sub} and increase of Q. At high ΔT_{sub} of 50°C and low Q of 4 kW favoring nucleate boiling, the flow oscillations are mainly due to bubble inception and bubble collapse. Estimation of correlation coefficients μ indicates that W_{loop}-time series are better correlated with p_{Hi}-time series (higher magnitude of μ) compared to that with Δp_H-time series at low Q and high ΔT_{sub}. Table 5 presents μ for W_{loop}-p_{Hi} and W_{loop}-Δp_H at different Q and ΔT_{sub}. Therefore, the role of Δp_H or friction (hydrodynamics) does not play significantly at the condition of low Q and high ΔT_{sub}. With decrease in ΔT_{sub} and increase of Q, the magnitude of μ for W_{loop}-Δp_H increases and the role of friction dominates.

Effect of inlet subcooling on flow oscillations

Here, we present our experimental results that the amplitude and the frequency of W_{loop}-oscillations increase as ΔT_{sub} is decreased (the cold-leg temperature is increased) at a given Q. The number of small peaks (low-amplitude oscillations) between two large peaks (corresponding to fundamental frequency) increases as ΔT_{sub} is increased. Figures 9a–c present the oscillations of W_{loop} at $\Delta T_{sub} = 50$, 40, and 30°C, respectively, for a given $Q = 4$ kW. The time-averages of W_{loop}-time series of a 1-h run at $Q = 4$ kW are found to be 27.43, 33.27, and 73.77 kg/h at ΔT_{sub} =50, 40, and 30°C, respectively. The significant increase of both average W_{loop} and amplitude of the flow oscillations at $\Delta T_{sub} = 30°C$ attributes to the formations of slugs or churns (confirmed by high-speed photography and direct visualization) that change boiling heat-transfer regime. A high ΔT_{sub} induces gravity-driven two-phase flow due to its low vapor quality flow in the HS and the expulsion of fluid (also known as fluid jet) from the HS reduces drastically. Consequently, the time period between two violent oscillations (dominant oscillations) increases with ΔT_{sub}; the dominant frequency of oscillations decreases. The same are also clearly shown in Figures 10a–c presenting PSDs of W_{loop}-oscillations at $Q = 4$ kW at $\Delta T_{sub} = 50$, 40, and 30°C, respectively. The small peaks at a relatively low ΔT_{sub} are quite a few while the large peaks are many, indicating that the number of the fundamental frequencies increases with decrease in ΔT_{sub}. It also appears from the increased number of fundamental frequencies that the oscillations may be chaotic at lower ΔT_{sub}. The increased number of small peaks at a high ΔT_{sub} is due to the bubbly flows (small bubbles in large volume of liquid). High subcooling hinders the bubble growth and the formation of large bubbles or slug bubbles takes place at a long time period.

Table 5. The Correlation Coefficient of $W_{loop} - p_{Hi}$ and $W_{loop} - \Delta pH$

Q (kW)	ΔT_{sub} (°C)	μ (W_{loop}-p_{Hi})	μ ($W_{loop} - \Delta p_H$)
4.0	50	−0.470	0.051
	40	−0.075	0.320
	30	−0.137	0.324
5.0	50	−0.149	0.332

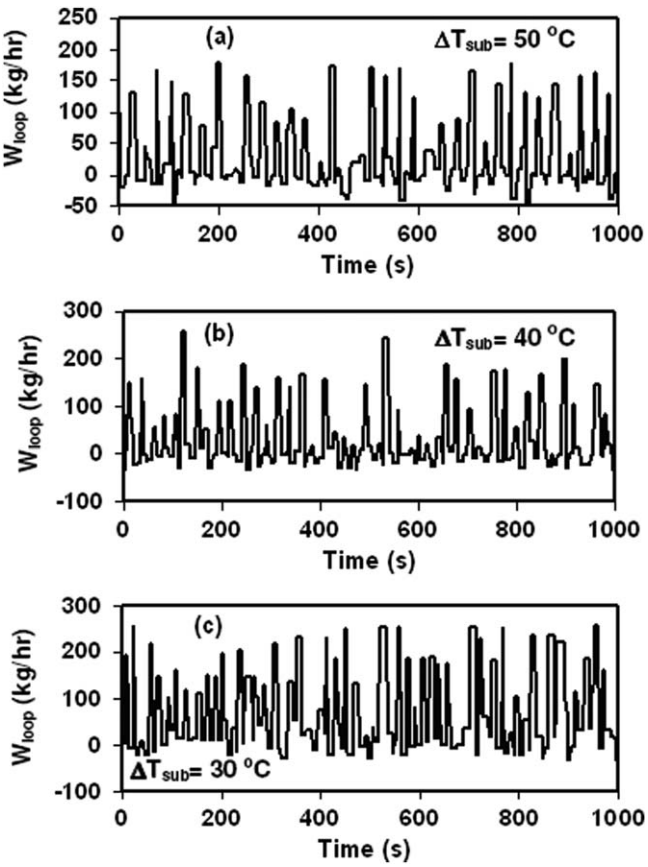

Figure 9. Effect of ΔT_{sub} on oscillations of W_{loop} at $Q = 4$ kW.

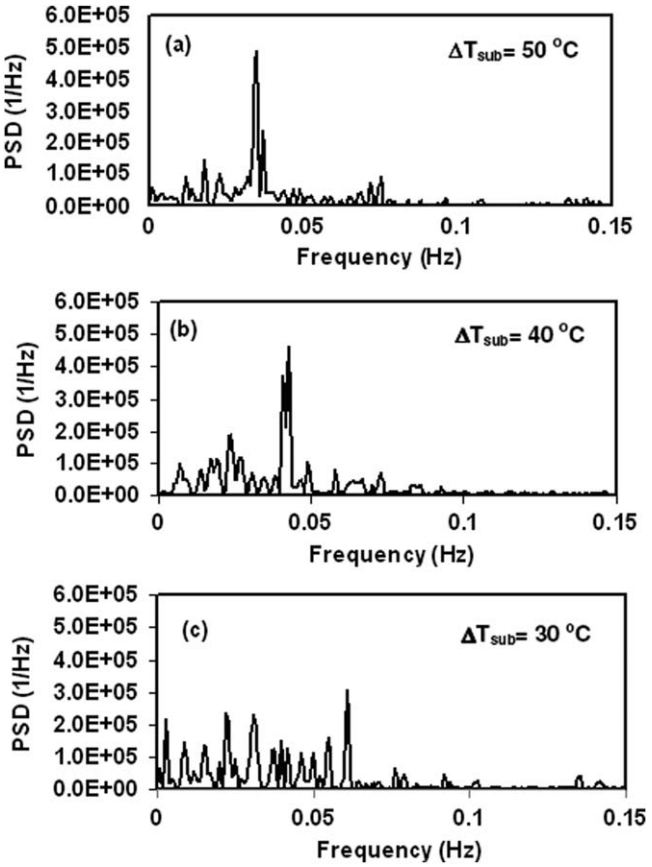

Figure 10. Effect of ΔT_{sub} on PSDs of oscillations of W_{loop} at Q =4 kW.

In our experiments, the flow variables were recorded at the rate of 0.5 Hz within the limit of our data logger, which is much less than the frequency of individual class of bubbles. Several classes of bubbles are observed due to their varied sizes (small or big) and shapes of the bubbles (spherical bubbles, mushroom shaped bubbles, slug bubbles, etc.). The peaks of the PSDs of p_{Hi}^{+} in Figure 8 are the signature of several classes of bubbles. From the power spectrums of the loop flow rate, the bubble frequencies were not obtained; rather the dominant frequency, as in Figure 10, gives the frequency of jet flow or expulsion of the vapor-liquid. The jet frequency was found to be very close to the frequency of big slug or mushroom-shaped bubbles observed through high-speed videos. The frequency increases with decrease in ΔT_{sub} and the slugs form more frequently. However, the power (amplitude) at the dominant frequency for the PSDs of p_{Hi}^{+} in Figure 8 implies how big the bubble is. As Q increases, the amplitude of p_{Hi}-oscillations increases due to the formation of larger bubbles.

Table 6 presents the effect of ΔT_{sub} on the dominant frequencies and their harmonics derived from the PSDs at $Q = 4$ kW. It is evident from Table 6 that the dominant frequency decreases with ΔT_{sub}. The harmonics of the dominant frequency (0.035 Hz) are 0.072 and 0.104 Hz at $\Delta T_{sub} = 50°C$. The dominant frequency and its harmonics at $\Delta T_{sub} = 40°C$ are also presented. But the strength of the harmonics is less whereas the strength of the dominant oscillations (0.043 Hz) is higher. At $\Delta T_{sub} = 30°C$, the four fundamental frequencies (0.061, 0.031, 0.022, and 0.003 Hz) are observed.

Table 7. Hurst Exponent of the Time Series of Loop Flow Rate

Q (kW)	ΔT_{sub} (K)	Hurst Exponent (H)
4.0	50	0.71 (persistent)
	40	0.67 (persistent)
	30	0.57 (close to random walk)
5.0	50	0.75 (persistent)
	40	0.63 (persistent)
	30	0.52 (close to random walk)

We also estimated the Hurst exponent H in order to quantify the fractal dimension of the time series of W_{loop} at different Q and ΔT_{sub}. In fact, H ($0 \le H \le 1$) reveals the persistent nature or antipersistent nature of a time series; the persistent nature dominates as H approaches to 1.0. Hurst[19] developed a statistical method to quantify H for a chaotic time series. H is estimated based on the following power-law relation of the rescaled range R/S (range/standard deviation) with the time scale τ of the observations

$$\frac{R}{S} = C\tau^{H} \tag{1}$$

where, C is constant. H is estimated from the slope of ln (R/S) vs. lnτ straight line. A time series with $H = 0.5$ is a random walk (Brownian or stochastic noise) and is independent. The time series having $0 < H < 0.5$ becomes antipersistent. H of a persistent series or black noise ranges from 0.5 to 1.0. A positive correlation exists in the persistent time series and it becomes stronger as H approaches to 1.0. The detailed computational algorithm for estimating H is available in the article of Hurst.[19] The values of H for the W_{loop}-time series, listed in Table 7, were estimated with the length of time series $N = 1000$ (number of data points) and the subperiods $n = 10$–500 at different ΔT_{sub} and Q. To confirm the converged value of H, we computed with N = 500, 900, 1000, and 1800, and obtained H with negligible difference. For example, at $\Delta T_{sub} = 30°C$ and $Q = 4$ kW, the values of H are 0.571, 0.564, 0.569, and 0.563 for $N = 500$, 900, 1000, and 1800 respectively. However, H for the time series ranges from 0.52 to 0.75 depending on Q and ΔT_{sub} indicating that the chaotic time series is deterministic ($H > 0.5$) and persistent (the time series can be predicted). However, at a given Q, the predictability of the W_{loop}-time series increases with increase in ΔT_{sub}. The value of H decreases to about 0.5 as ΔT_{sub} is decreased to 30°C; the signals become Brownian

Table 6. Effect of Inlet Subcooling on the Frequency of W_{loop} Oscillations at 4 kW

ΔT_{sub} (°C)	50.0			40.0			30.0			
Strength (Hz^{-1})	480,700	238,600	103,100	458,100	369,100	186,300	309,000	235,200	232,600	214,400
Fundamental frequency (Hz)	0.035	0.037	0.023	0.043	0.041	0.023	0.061	0.031	0.022	0.003
Harmonic frequency (Hz)	0.072	0.075	0.047	0.086	0.081	0.047	0.121	–	–	–
Harmonic frequency (Hz)	0.104	0.112	0.069	0.126	0.123	0.07	–	–	–	–

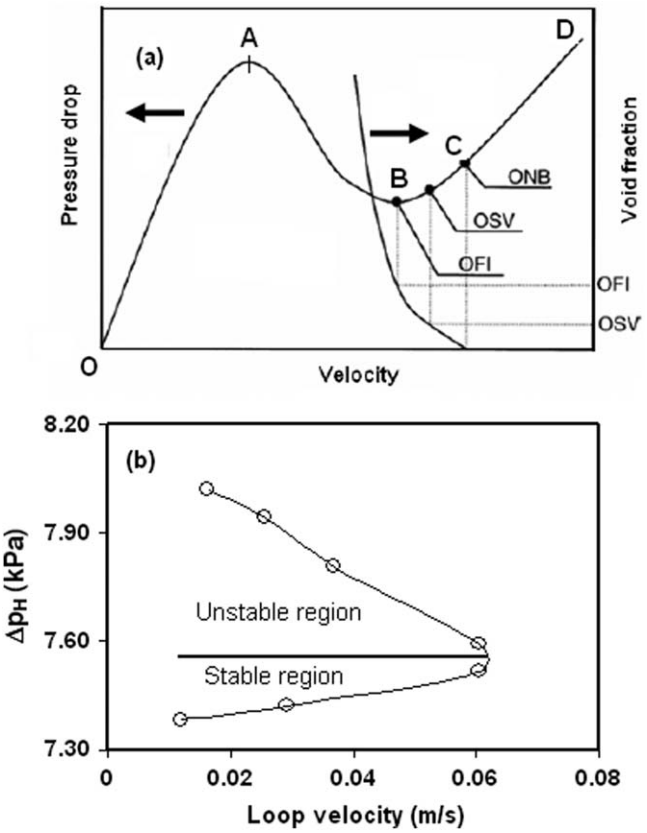

Figure 11. (a) Δp-velocity characteristics in forced-flow boiling indicating ONB, OSV, OFI.[1]

(b) Δp_H – loop velocity characteristics in NCBL in our experiments.

(which is difficult to predict) with decrease in ΔT_{sub}. $H = 0.72$–0.75 at $\Delta T_{sub} = 50°C$ indicates that the time series becomes more predictable and can be better correlated at a high ΔT_{sub}. Table 7 also shows that the effect of Q on H is not significant, although a small improvement in the predictability with increase in Q is noted at $\Delta T_{sub} = 50°C$. Our H-values are comparable with those of Wang et al.[20] who found H to be 0.72–0.87 for bubbly flow and 0.67 for annular flow. The overall comparison also clearly mentions that the oscillation is more chaotically complex at a higher Q and at a lower ΔT_{sub}.

Onset of flow instability

To derive a mechanism of the onset of flow instability (OFI) observed in our NCBL, it is very important to review the existing mechanisms of bubble nucleation. The nucleation is primarily initiated by the active sites (cavities) and the wall superheating.[21,22] With the increase in heat flux q″, T_w increases and exceeds T_{sat} at the local pressure. The profile of T_l is usually assumed to be linear through the thermal boundary layer. The nucleation takes place when T_l over the top of the bubble exceeds the temperature necessary for the nucleation at equilibrium. However, we found two criteria for forced-flow subcooled boiling oscillations in literatures—one based on wall superheating or bubble growth[23] and the other based on hydrodynamics.[2] The literatures[24–26]on the bubble growth in tube suggest that the growth or collapse of bubbles over the cross section of a tube is due to the temperature gradient across the radius of the tube. The source theory[26]derives the following average growth rate of steam bubbles

$$\dot{R}_{avg} = \frac{\sqrt{\pi\kappa}}{r_i^2\sqrt{t}} \frac{\rho_l c_{pl}}{\rho_g h_{fg}} \int_0^{r_i} (T_l - T_{sat})\ r dr \tag{2}$$

Equation 2 implies that if the liquid temperature T_l is higher than the interface temperature T_{sat} (usually assumed to be the saturation temperature at the local pressure), the liquid gets superheated and the bubble starts to form and grow; otherwise, the bubble starts to collapse. However, the formulation of Eq. 2 requires estimating bubble growth parameter ζ given by Eq. 3 obtained based on the assumption of asymptotic bubble growth

$$\zeta = \frac{\sqrt{\pi}}{2} \frac{\rho_l c_{pl}}{\rho_g h_{fg}} (T_l - T_{sat}) \tag{3}$$

The above equation explains the faster bubble growth at a higher ΔT_{sat}. Our direct observations and high-speed video make sure that the large bubbles form just before the onset of flow oscillations. On the other hand, the bubble formation is favored by the conditions at which $\dot{R}_{avg}$ becomes zero. $\dot{R}_{avg}$ is greater than zero for a net bubble growth. So, one can consider $\dot{R}_{avg} = 0$ to be the necessary condition of OFI from which Eq. 4 is obtained

$$\int_0^{r_i} (T_l - T_{sat})\ r dr = 0 \tag{4}$$

Equation 4 must be satisfied for OFI to occur in subcooled boiling in a round tube.

Mechanism of OFI in the present NCBL

For a fully developed single-phase flow under forced convection at q″, the total pressure drop Δp decreases with decrease in velocity v. On gradual reduction of v (the pressure drop also decreases), the onset of nucleate boiling (ONB) and the onset of significant voids (OSV) are detected. The same are indicated in Figure 11a for the $\Delta p - v$ curve for a forced-flow boiling channel. Further reduction of v causes Δp to increase through a minimum point on the curve. OFI occurs at the minimum point. The flow instability becomes stronger as we reduce v further to the point on the curve with a negative slope. The section "D to C" indicates stable single-phase liquid, "C to A" two phase, "B to A" unstable two-phase and "A to O" stable single-phase vapor. In some cases, the occurrence of multiple solutions and the instability threshold can be predicted using the steady-state equations of the process. The Ledinegg instability[2] is one such example that occurs in NCBL and forced-flow boiling channel. The conditions for this instability are given by

$$\frac{\partial(\Delta p_i)}{\partial v} \le 0 \quad (\text{for forced}-\text{flow boiling channel}) \tag{5a}$$

$$\frac{\partial(\Delta p_i)}{\partial v} - \frac{\partial(\Delta p_d)}{\partial v} \le 0 \quad (\text{for NCBL}) \tag{5b}$$

Δp_i is the internal pressure loss in the system and Δp_d is the driving head due to buoyancy. Δp_i includes the losses due to friction and acceleration in the HS, riser and DC. Δp_d $(= \Delta p_{d,DC} - \Delta p_{d,HS} - \Delta p_{d,riser})$ counts for the gravity heads in the DC, the HS and the riser. Δp_d plays a primary role in

inducing natural circulation in NCBL. With this basis, we have computed heater pressure drop Δp_H-loop velocity characteristic curve for our NCBL. The curve is presented in Figure 11b. Both the stable region and the unstable region have been indicated in the figure. In our experimental range of q″, the HS substantially contributes to the total frictional pressure drop compared to the DC and the riser.

Role of Wall Superheat in OFI. In our NCBL, we note that W_{loop}-oscillations strongly depend on ΔT_{sat}. We plotted the first 100-s history of ΔT_{sat} (calculated at the exit of the HS), Δp_H and W_{loop} at $Q = 4.0$ kW and $\Delta T_{sub} = 50°C$. Figure 12a shows the time history of ΔT_{sat} and Δp_H while Figure 12b shows the time history of W_{loop}. The figures indicate that the peaks of W_{loop}-oscillations appear when ΔT_{sat} exceeds a critical value that favors the formation of significant voids. At the critical value, a sharp decrease of Δp_H and an increase of W_{loop} are noticed. It clearly indicates that hydrodynamic instability is initiated by the effect of wall superheat that forms the thermodynamic basis. Kamil et al.[27] also experimentally reported that ΔT_{sat} plays a significant role in the formation of large bubbles and thereby large turbulent eddies during nucleate boiling in a natural circulation reboiler.

It is also evident from the figures that W_{loop} mostly oscillates in-phase with ΔT_{sat}. With increase in ΔT_{sat}, Δp_H decreases. It should be mentioned that the oscillations of ΔT_{sat} are due to the changes of saturation temperature because of the oscillations of the pressure at the exit of heater (wall temperature was observed to remain almost unchanged). At higher Q (5 kW), ΔT_{sat} sometimes oscillates in out-of-phase mode with W_{loop} as shown in Figures 13a, b, for example, at 54 and 74 s. It is also very interesting to note that the dominant frequency and its harmonics of

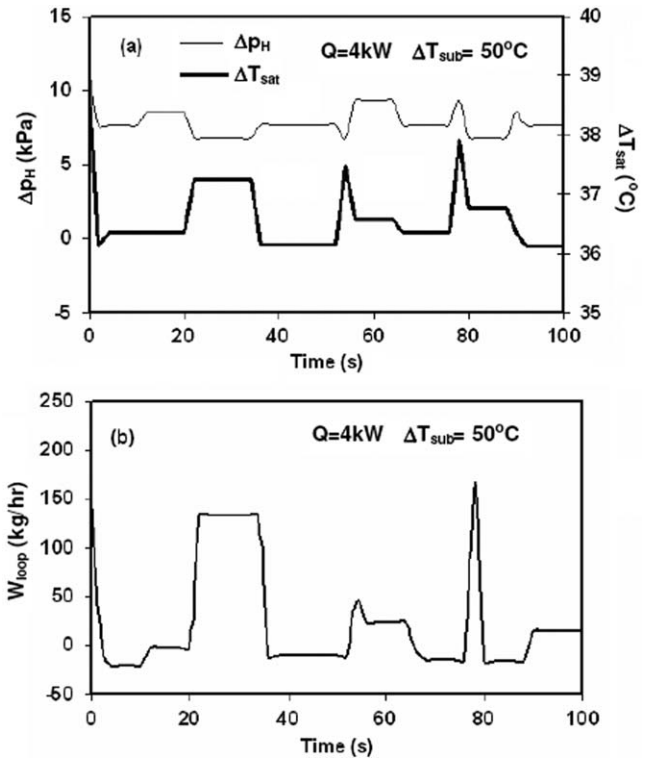

Figure 12. (a) Time evolution of ΔT_{sat} and Δp_H (b) time evolution of W_{loop} at $Q = 4$ kW and $\Delta T_{sub} = 50°C$.

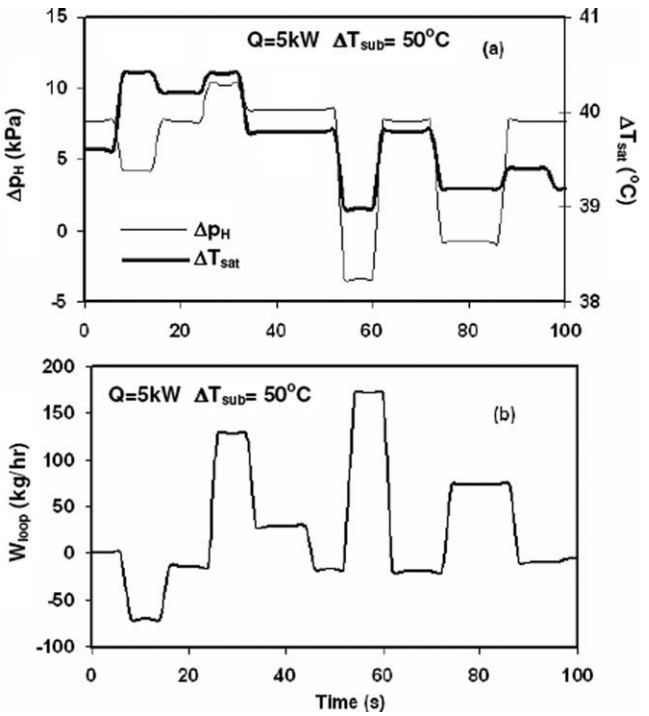

Figure 13. (a) Time evolution of ΔT_{sat} and Δp_H (b) time evolution of W_{loop} at $Q = 5$ kW and $\Delta T_{sub} = 50°C$.

W_{loop} (0.035, 0.072, and 0.104 Hz) and those of p_{Hi}^{+} (0.036, 0.072, and 0.108 Hz) at $Q = 4$ kW and $\Delta T_{sub} = 50°C$ are very close. It clearly shows that the flow instability originates due to the effect of bubble dynamics.

Conclusions

Our studies reveal that the hydrodynamic instability initiates due to the effect of ΔT_{sat}. An increase of ΔT_{sat} intensifies the formation of vapor slugs. The flow instability originates due to bubble dynamics (bubble growth and bubble collapse that form thermodynamic basis) and it strongly depends on the departure bubble frequency; the thermodynamic effect eventually induces the vigorous hydrodynamic oscillations. The oscillations of W_{loop} at $Q = 4$ kW and $\Delta T_{sub} = 50°C$ have been observed to be coupled with p_{Hi}; their frequencies are same.

Here, we summarize our major findings as follows

1. The scaling ratio of the geometry of NCBL affects the stability of the loop. A lower Ω of our NCBL imparts to the extended flow termination and flow reversal. The decrease in Φ causes the increased p_{Hi}-fluctuations (bubble dynamics) and the increased reverse flow.
2. The oscillations at low Q and high ΔT_{sub} are very similar to the geysering instability. The geysering oscillations, as we observe here, are mainly quasiperiodic at $Q = 3$ kW and chaotic at $Q = 4$ and 5 kW.
3. PSDs of p_{Hi} and W_{loop} reveal that the oscillations gradually change from the quasiperiodic ones to the chaotic ones with increase in Q and with a decrease in ΔT_{sub}. The dominant frequency increases with increase in Q and with decrease in ΔT_{sub}. At a higher Q, a higher dimensional chaotic behavior is observed through attractor reconstruction.

4. Estimations of H conclude that W_{loop}-time series are persistent and can be better correlated at a high ΔT_{sub}, whereas they gradually gain Brownian noise at low ΔT_{sub}. The variations of H confirm that the effect of ΔT_{sub} on the instability dominates over the effect of Q.

Acknowledgments

We gratefully acknowledge Prof. P. Ray, University of Calcutta, for valuable discussions and the peer reviewers of this manuscript for their valuable suggestions for improving the technical content and presentation. We also appreciate the financial support of SERC, Department of Science and Technology (DST), India (Sanction No. SR/S3/CE/089/2009) for this work.

Notation

C = proportionality constant in Eq. 1
c_p = heat capacity, J/kg-K
D = diameter, m
g = acceleration due to gravity, 9.81 m/s^2
h = enthalpy, J/kg
H = Hurst exponent
k = thermal conductivity, W/m-K
L = length, m
m = Number of subperiods of length n
N = length of time series
p = pressure, kPa
p_{loop} = loop pressure, kPa
Δp = pressure drop, N/m^2
q$''$ = heat flux, kW/m^2
Q = heater power, kW
r = radius/radial distance, m
R_i = range for ith subperiod
$\dot{R}$ = rate of change of bubble radius
S_i = standard deviation for ith subperiod in Eq. 1
t_{boil} = time for inception for flow instability, s
T = temperature, °C
ΔT_{sub} = inlet subcooling, °C
ΔT_{sat} = wall superheat, °C
V_{loop} = loop volume, m^3
v = velocity, m/s
W_{loop} = loop flow rate, kg/h

Greek letters

α = void fraction, dimensionless
ζ = bubble growth parameter
Δ = differential
κ = constant in Eq. 2
Φ = initial liquid volume, m^3
μ = correlation coefficient
ρ = density, kg/m^3
τ = time scale in Eq. 1
Ω = ratio of riser length to HS-length

Subscripts

avg = average
d = driving force
DC = down comer
g = vapor phase
fg = phase change (saturated liquid to vapor)
H = heater
HS = heated section
i = inlet /internal
l = liquid phase
o = outlet
riser = riser section
sat = saturation/superheat
sub = subcooled
w = wall

Superscript

+ = dimensionless

Abbreviations

BWR = boiling water reactor
CLTC = cold leg temperature controller
DC = down comer
DWO = density-wave oscillation
EFM = electromagnetic flow meter
HS = heated section
LOCA = loss of coolant accident
NCBL = natural circulation boiling loop
OFI = onset of flow instability
ONB = onset of nucleate boiling
OSV = onset of significant void
PC = pressure controller
PSD = power spectral density

Literature Cited

1. Boure JA, Bergles AE, Tong LS. Review of two-phase flow instability. *Nucl Eng Des*. 1973;25:165–192.
2. Ledinegg M. Instability flow during natural forced circulation. *Die Warme*. 1938;61:891–898.
3. Wissler E, Isbin HS, Amudson NR. Oscillatory behavior of a two-phase natural circulation loop. *AIChE J*. 1956;2:157–162.
4. Chexal VK, Bergles AE. Two phase instabilities in a low pressure natural circulation loop. In: Proceedings of the 13th National Heat Transfer Conference of AIChE Symposium series, Vol. 69. Denver, CO, 1973:37–45.
5. Fukuda K, Kobori T. Classification of two-phase flow stability by density wave oscillation model. *J Nucl Sci Technol*. 1979;16: 95–108.
6. Aritomi M, Chiang JH, Nakahashi T. Fundamental study on thermo-hydraulics during start-up in natural circulation boiling water reactor (I), Thermo-hydraulic instabilities. *J Nucl Sci Technol*. 1992;29:631–641.
7. Wang SB, Wu JY, Pan C, Lin WK. Thermal-hydraulic oscillations in a low pressure two-phase natural circulation loop at low powers and high inlet subcoolings. In: *The 4th International Topical Meeting on Nuclear Thermal Hydraulics*, Operations and Safety. Taipei, Taiwan, April 6–8, 1994.
8. Jiang SY, Yao MH, Bo JH, Wu SR. Experimental simulation study on startup of the 5 MW nuclear heating reactor. *Nucl Eng Des*. 1995;158:111–123.
9. Kyung IS, Lee SY. Periodic of flow excursion in an open two-phase natural circulation loop. *Nucl Eng Des*. 1996;162:233–244.
10. Hsieh CC, Wang SB, Pan C. Dynamic visualization of two-phase flow patterns in a natural circulation loop. *Int J Multiphase Flow*. 1997;23:1147–1170.
11. Nayak AK, Jain V, Vijayan PK, Saha D, Sinha RK. Experimental investigation on the flow instability behavior of a multichannel boiling natural circulation loop at low pressures. *Exp Therm Fluid Sci*. 2010;34:776–787.
12. Paruya S, Bhattacharya P. Simulation of oscillations in boiling flow in a natural circulation evaporator. *Chem Eng Commun*. 2009;196: 362–390.
13. Boure JA. Oscillatory two phase flow. In: Ginoux JJ. *Two-Phase Flows and Heat Transfer with Application to Nuclear Reactor Design Problems*. Washington: Hemisphere Pub. Corp., 1978.
14. Marcel CP, Rohde M, Van Der Hagen THJJ. Experimental investigations on flashing-induced instabilities in one and two-parallel channels: a comparative study. *Exp Therm Fluid Sci*. 2010;34:879–892.
15. Paruya S, Saha AK, Bhattacharya P. Validations of thermohydraulic models for geysering in a natural circulation loop using an impedance needle probe. *Ind Eng Chem Res*. 2009;48:2020–2033.
16. Yadigaroglu G. Two-phase flow instabilities and propagation phenomena. In: Delhaye JM, Giot M, Riethmuller ML. *Thermodynamics of Two-Phase Systems for Industrial Design and Nuclear Engineering*. New York: McGraw-Hill, 1981:353.
17. Takens F. Detecting Strange Attractors in Turbulence. In: Rand DA, Young LS. *Dynamical Systems and Turbulence, Lecture Notes in Mathematics*. Berlin: Springer-Verlag, 1981:366.
18. Leibert W, Schuster HG. Proper choice of delay time for the analysis of chaotic time series. *Phys Lett A*. 1991;142:107–111.

19. Hurst HE. Long term storage capacity of reservoirs, *Trans Am Soc Civil Eng*. 1952;116:770–776.
20. Wang SF, Mosdorf R, Shoji M. Nonlinear analysis on fluctuation feature of two-phase flow through a T-junction, *Int J Heat Mass Transf*. 2003;46:1519–1528.
21. Forster HK, Zuber N. Dynamics of vapor bubbles and boiling heat transfer. *AIChE J*. 1955;1:531–535.
22. Davis WJ, Anderson GH. The incipience of nucleate boiling in forced convection flow. *AIChE J*. 1966;12:774–780.
23. Jeglic FA, Grace TM. Onset of flow oscillations in forced flow subcooled boiling. In: NASA Technical Note TN D-2821, Cleveland, Ohio: Lewis Research Center, 1965.
24. Scriven LE. On the dynamics of phase growth. *Chem Eng Sci*. 1959; 10:1–13.
25. Plesset MS, Zwick SA. The growth of vapor bubbles in superheated liquids. *J Appl Phys*. 1954;25:493–500.
26. Clark JA, Yang WJ. On the application of the source theory to the solution of problems involving phase change. i. growth and collapse of bubbles. *J Heat Transf*. 1964;86:207–212.
27. Kamil M, Shamsuzzoha M, Abdul Hakeem M. Analysis of incipience of nucleate boiling in a reboiler tube. *AIChE J*. 2007;53:39–50.

Manuscript received Mar. 6, 2013, and revision received Sept. 4, 2013.